Efficient electrothermal actuation of multiple modes of high-frequency nanoelectromechanical resonators

I. Bargatin, I. Kozinsky, and M. L. Roukes[a)]

Kavli Nanoscience Institute, California Institute of Technology, Pasadena, California 91125
and Condensed Matter Physics, California Institute of Technology, Pasadena, California 91125

The authors observed resonances from multiple vibrational modes of individual silicon-carbide-based nanomechanical resonators, covering a broad frequency range from several megahertz to over a gigahertz. The devices are actuated thermoelastically in vacuum at room temperature using localized Joule heating in a device-integrated metal loop. Their motion is detected piezoresistively using signal downmixing in a similarly integrated metal piezoresistor. The frequencies and amplitudes of the observed resonant peaks are in good agreement with the results from theoretical modeling and finite-element simulations. © *2007 American Institute of Physics*. [DOI: 10.1063/1.2709620]

The recent interest in nanoelectromechanical systems (NEMSs) is motivated by a wide range of possible applications, including advanced imaging,[1] zeptogram-range mass sensing,[2] attonewton-range force sensing,[3] and quantum effects in mechanical devices.[4,5] A continuing challenge in the field is efficient actuation and detection of NEMS motion, since existing methods often scale poorly to smaller dimensions. A number of techniques have been explored recently to address this challenge. Magnetomotive[6] and capacitive[7] techniques provide a way to actuate and detect motion simultaneously. There are also stand-alone methods for both actuation, such as thermoelastic[8] and piezoshaker[9,10] actuation; and detection, such as piezoresistive[9–11] and optical,[3,8] as well as detection techniques based on motional changes in the electronic properties of single electron transistors[4,12] and nanotubes.[13] Each of these techniques has advantages as well as limitations. For example, the magnetomotive technique typically requires large magnetic fields, whereas optical techniques require careful alignment of optical components.

For the experiments reported here, we combine piezoresistive downmixing detection, developed earlier in Ref. 9, with thermoelastic actuation due to localized Joule heating of a metallic resistor. Figure 1(a) shows one of the doubly clamped beam resonators used in the experiments. The beams were made from a single-crystal silicon carbon (3*C*-SiC) thin film by multiple aligned steps of e-beam lithography, thin film evaporation, lift-off, and reactive plasma etching.[14] They had nominal lengths between 4 and 24 μm, a width of 400 nm, and a thickness of 80 nm. Two different thin metal film loops were patterned near the two ends of the beam. The 80-nm-thick, 100-nm-wide loop was patterned from thermally evaporated gold and formed a part of the thermoelastic bilayer actuator [right inset of Fig. 1(a)]. The thinner piezoresistor loop was patterned from a 30-nm-thick metal layer created by evaporating a 60%–40% gold palladium alloy [left inset of Fig. 1(a)]. It consisted of 250-nm-long, 50-nm-wide legs connected by a larger pad [left inset of Fig. 1(a)]. A 2-nm-thick chromium adhesion layer was used in both cases. Typical resistances of metal

loops were 30 Ω for the actuation loop and 300 Ω for the detection loop.

Thermoelastic actuation of bilayer structures has long been employed, for example, in thermostats,[15] and relies on the fact that the coefficient of linear thermal expansion varies for different materials. For gold and silicon carbide, $\alpha_{Au} \approx 12 \times 10^{-6}$ K^{-1} and $\alpha_{SiC} \approx 4.8 \times 10^{-6}$ K^{-1}, respectively. Local heating of the gold actuation loop in our devices therefore results in nonuniform expansion and thermal stresses that tend to flex the beam toward the substrate. If the temperature changes periodically at the resonance frequency of one of the mechanical modes of the resonator, the amplitude of deflection will be greatly enhanced due to the large quality factors of nanomechanical resonators. The thermoelastic mechanism has been used previously to actuate microelectromechanical resonators by local Joule heating[16] as well as NEMS resonators by local laser heating.[8] These previous studies used optical detection. In contrast, our technique offers the convenience of fully integrated, purely electronic actuation and detection, as well as the ability to detect doz-
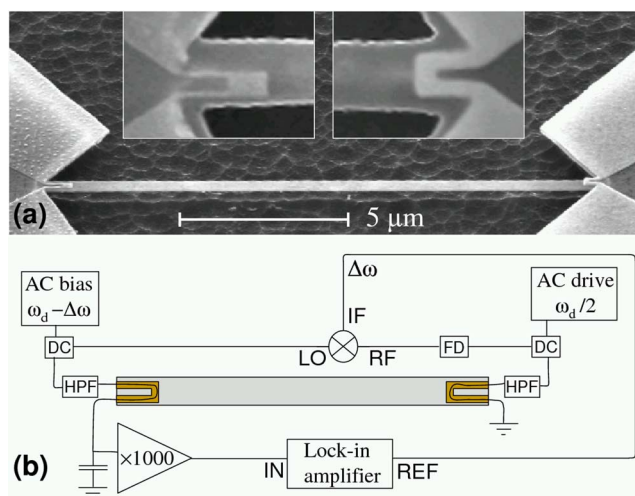

FIG. 1. (Color online) (a) Scanning electron micrograph of one of the devices used in the experiments (oblique view). The insets show top-view closeup images of the detection (left) and drive (right) metal loops. (b) Schematic of the experimental setup: DC denotes directional coupler, FD frequency doubler, and HPF high-pass filter.
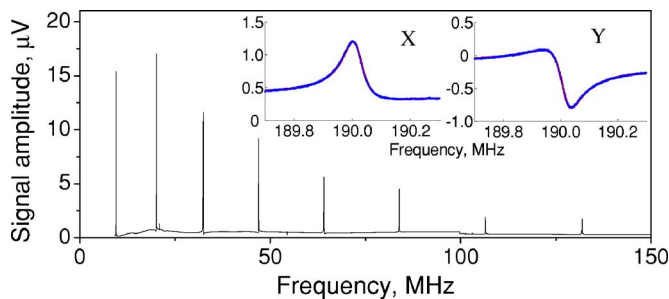
a)Electronic mail: roukes@caltech.edu

FIG. 2. (Color online) Raw signal, referred to the preamplifier input, from a 16-μm-long beam. The root-mean-square amplitudes of the drive and bias voltages are 22 and 118 mV, respectively. The inset shows both quadratures of the resonant response of the tenth out-of-plane mode (not shown in main panel) and the almost indistinguishable Lorentzian fit to the data.
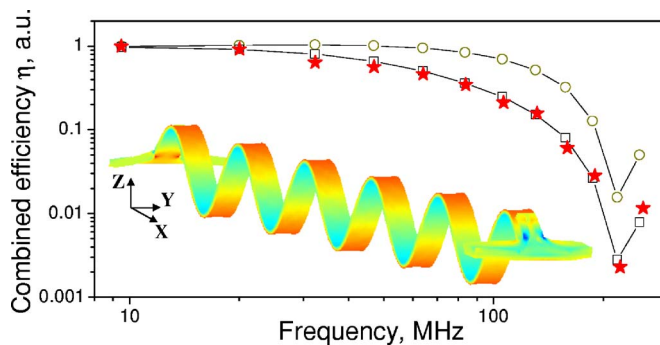

FIG. 3. (Color online) Efficiency of electrothermal drive and piezoresistive detection, normalized to that of the fundamental mode, for the first 12 out-of-plane modes of the 16-μm-long beam. The stars show experimental data, while the connected symbols show the results of finite-element simulations excluding (circles) and including (squares) the effect of 40 MHz thermal rolloff. The inset shows the predicted shape of the 11th out-of-plane mode.

ens of vibrational resonances of the same NEMS structure.

Figure 1(b) shows a schematic of the experimental setup. Periodic temperature variations at drive frequency ω_d are induced by applying a drive voltage at half the frequency $\omega_d/2$ to the actuation loop. An ac bias voltage of frequency $\omega_d - \Delta\omega$ is applied to the detection loop on the other end of the beam. The downmixed signal voltage at frequency $\Delta\omega$ generated in the piezoresistor[9] is then amplified by a high-input-impedance preamplifier and detected with a lock-in amplifier. Fractions of the drive and bias signals are split off with directional couplers and fed to a broadband frequency doubler and mixer to produce the reference signal for the lock-in amplifier. Commercial 3 MHz high-pass filters, followed by 10 dB attenuators (not shown), are inserted in the bias and drive channels to reduce the parasitic background and noise in the detected signal.

Figure 2 shows the magnitude of the raw signal from a 16-μm-long beam detected as both the drive and bias voltages are swept over a very wide range of frequencies while keeping the downmixed frequency constant at 95 kHz. The large peaks correspond to the first eight out-of-plane flexural modes of the beam. The small peak near the second large peak corresponds to the first in-plane mode. On resonance, both quadratures of the lock-in signal fit the Lorentzian curve shape very well (inset of Fig. 2). The noise floor of ≈ 3 nV/Hz$^{1/2}$ is largely due to the Johnson noise of the piezoresistor. The small background signal originates from the parasitic coupling between bias, drive, and detection channels and the slight nonlinearity of the piezoresistor and preamplifier response.

Table I lists the frequencies of the first 17 vibrational modes of the 16-μm-long device predicted from FEMLAB finite-element simulations, and also shows their measured frequencies and quality factors determined from Lorentzian fits. Discrepancies between predicted and observed frequen-

cies do not exceed a few percent for all modes if the intrinsic strain, which presumably arises during fabrication of multilayer structures, is taken into account. The agreement is excellent for the lower modes and deteriorates slightly only for the highest modes. We attribute this to the difficulty of realistically modeling the imperfect clamping of our beams at their ends. We observe many more resonance peaks above the resonance frequency of the 12th out-of-plane mode, up to a resonance at 1.094 GHz; however, these resonance peaks become progressively smaller and some of them overlap, which makes it difficult to identify the nature of the corresponding modes and fit the resonance peaks to Lorentzian curves.

Piezoresistive detection of motion relies on variation ΔR in the resistance of the conducting loop, which in metals is mainly caused by the changes in the shape of the conductor.[10] The amplitude of the downmixed piezoresistive signal is approximately $V_s \approx V_b \Delta R / (2R) = V_b g \langle \varepsilon_{xx} \rangle / 2$, where V_b is the amplitude of the applied ac bias voltage, g is the effective gauge factor of the piezoresistor, and $\langle \varepsilon_{xx} \rangle$ is the average longitudinal strain in the displacement transducer (coordinate axes are shown in the inset to Fig. 3). If the temperature variations induced by the actuation voltage are sinusoidal and resonant with the vibrational mode n at frequency ω_n, the strain distribution in the piezoresistor is mostly determined by the corresponding mode shape, $\mathbf{u}^{(n)}(\mathbf{r})$, which specifies the vector displacement $\mathbf{u}$ of the infinitesimal volume element located at radius vector $\mathbf{r}$. The amplitude of motion in steady state can then be deduced from the condition of balance between the energy dissipated by the nanomechanical resonator due to its finite quality factor and the mechanical work done by the time-varying thermal stresses induced in the drive loop:

TABLE I. Predicted, f_{pred}, and experimental, f_{exp}, resonance frequencies, as well as quality factors in vacuum, Q_{exp}, for the lowest twelve out-of-plane (out) modes and lowest five in-plane (in) modes of a 16-μm-long beam. In simulations, we assume the following material properties for the SiC layer: Young's modulus of 430 GPa, Poisson ratio of 0.3, mass density of 3.2 g/cm^3, (Ref. 17), and intrinsic tensile strain of 2.8×10^{-4}. The strain value was varied to obtain the best fit to the experimental frequencies.

Mode	1 out	2 out	1 in	3 out	4 out	2 in	5 out	6 out	3 in	7 out	8 out	9 out	4 in	10 out	11 out	5 in	12 out
f_{pred} (MHz)	9.48	20.0	20.7	32.3	46.9	54.3	64.1	83.8	103	106	131	158	166	187	219	244	252
f_{exp} (MHz)	9.52	20.0	20.8	32.3	46.8	54.0	63.9	83.5	103	107	132	160	167	190	223	243	258
Q_{exp}	12000	7750	3110	5570	4410	2630	3620	3220	2210	2950	2700	2510	1740	2190	1970	1760	1660

$$\frac{c_n \omega_n^2}{\pi Q_n} \int \rho(\mathbf{r}) \mathbf{u}^{(n)}(\mathbf{r})^2 d\mathbf{r} = \int \sum_{i,j} \sigma_{ji}(\mathbf{r}) \frac{\partial \mathbf{u}_i^{(n)}(\mathbf{r})}{\partial \mathbf{r}_j} d\mathbf{r}. \qquad (1)$$

Here the summation is over all spatial coordinates and the integrals are over the volume of the bilayer resonator, c_n is the normalized mode amplitude, $\rho(\mathbf{r})$ the local mass density, and $\sigma_{ji}(\mathbf{r})$ the amplitude of the thermal stress tensor. If we assume, for simplicity, that gold and silicon carbide components are elastically isotropic then $\sigma_{ii}(\mathbf{r}) \approx 3\alpha(\mathbf{r})\Delta T(\mathbf{r})B(\mathbf{r})$, where $\alpha(\mathbf{r})$ is the thermal coefficient of linear expansion, $\Delta T(\mathbf{r})$ is the amplitude of temperature change, and $B(\mathbf{r})$ is the bulk modulus. Solving Eq. (1) for the mode amplitude c_n allows us to find the spatially averaged longitudinal strain in the piezoresistor $\langle \varepsilon_{xx} \rangle = c_n \langle \partial \mathbf{u}_x^{(n)}(\mathbf{r})/\partial x \rangle$ and hence the corresponding downmixed voltage signal.

For the higher flexural out-of-plane modes, the strain may change sign within the length of the actuation or detection loop (Fig. 3, inset), resulting in partial cancelation of the right-hand side integral in Eq. (1) and the detected strain average. To study these cancelation effects, we can introduce an empirical efficiency of the combined electrothermal drive and piezoresistive detection. Since the resonance amplitude a is normally proportional to the bias voltage V_b, drive voltage squared V_d^2, and the quality factor Q, we will define the efficiency as $\eta = a/(QV_d^2 V_b)$ so that it depends only on the strain and temperature distributions in the resonator. Figure 3 shows that this efficiency η generally decreases with the mode number and, in this device, dips sharply for the 11th out-of-plane mode due to almost complete cancelation of drive integral in Eq. (1). Note that for in-plane modes, the drive integral should cancel completely due to symmetry and the efficiency η should, in principle, be zero. In practice, real devices are never perfectly symmetric, and we find that the in-plane modes are easily detectable with increased drive voltages. However, the measured efficiencies for in-plane modes are typically one to two orders of magnitude smaller than the efficiencies of out-of-plane modes of similar frequencies.

The efficiency η additionally decreases with frequency because of the delayed response of the temperature to Joule heating. In order to be most effective, the temperature must follow the drive voltage (squared) instantaneously, but in reality it takes a thermal time constant τ_{th} for the temperature to equilibrate. Therefore, above a certain drive frequency, the induced temperature variations will roll off since the device acts as a thermal low-pass filter, and the efficiency of thermal drive will decrease accordingly. The thermal time constant estimated from fitting finite-element simulations for efficiency to the experimental data is $\tau_{th} = (2\pi \cdot 40 \text{ MHz})^{-1} \approx 4$ ns (Fig. 3). This number agrees with the theoretical estimate for τ_{th} we derive by directly considering the heat conduction dynamics in the bilayer actuator.

Electrothermal actuation and piezoresistive detection with large voltages can excessively heat the device. This becomes especially important for electrothermal drive above the thermal cutoff frequency, since only a fraction of the applied time-varying Joule heating power then results in useful periodic temperatures changes; the remainder simply raises the average temperature of the beam. While it is difficult to measure the temperature distribution of the beam directly, we can estimate the average temperature increase of the beam from the observed changes in resonance shapes at high applied voltages using separately determined temperature dependencies of resonance frequencies and Q factors. These measurements indicate that the devices are approximately one-tenth of kelvin hotter than the environment for every microwatt of dissipated Joule power. The majority of data collected in this experiment were thus taken with the beams only a few Kelvins hotter than the environment.

The combination of electrothermal actuation and piezoresistive detection thus provides a convenient and efficient all-electronic measurement technique for NEMS devices and will be beneficial in applications such as mass sensing, where obtaining data from multiple modes can improve the accuracy and speed of measurements.[18] Both thermal actuation and piezoresistive detection scale more favorably with the device dimensions than many alternative techniques, allowing future experiments with even smaller nanomechanical devices.

[1]S. Hosaka, K. Etoh, A. Kikukawa, and H. Koyanagi, J. Vac. Sci. Technol. B **18**, 94 (2000); T. Ando, N. Kodera, E. Takai, D. Maruyama, K. Saito, and A. Toda, Proc. Natl. Acad. Sci. U.S.A. **98**, 12468 (2001).
[2]Y. T. Yang, C. Callegari, X. L. Feng, K. L. Ekinci, and M. L. Roukes, Nano Lett. **6**, 583 (2006).
[3]D. Rugar, R. Budakian, H. J. Mamin, and B. W. Chui, Nature (London) **430**, 329 (2004).
[4]A. Naik, O. Buu, M. D. LaHaye, A. D. Armour, A. A. Clerk, M. P. Blencowe, and K. C. Schwab, Nature (London) **443**, 193 (2006).
[5]K. C. Schwab and M. L. Roukes, Phys. Today **58**(7), 36 (2005).
[6]A. N. Cleland and M. L. Roukes, Appl. Phys. Lett. **69**, 2653 (1996).
[7]P. A. Truitt, J. B. Hetzberg, C. C. Huang, K. L. Ekinci, and K. C. Schwab, Nano Lett. **7**, 120 (2007).
[8]N. V. Lavrik and P. G. Datskos, Appl. Phys. Lett. **82**, 2697 (2003); B. Ilic, S. Krylov, K. Aubin, R. Reichenbach, and H. G. Craighead, *ibid.* **86**, 193114 (2005); A. Sampathkumar, T. W. Murray, and K. L. Ekinci, *ibid.* **88**, 223104 (2006).
[9]I. Bargatin, E. B. Myers, J. Arlett, B. Gudlewski, and M. L. Roukes, Appl. Phys. Lett. **86**, 133109 (2005).
[10]M. Li, H. X. Tang, and M. L. Roukes, Nat. Nanotech. **2**, 114 (2007).
[11]J. A. Harley and T. W. Kenny, Appl. Phys. Lett. **75**, 289 (1999).
[12]R. G. Knobel and A. N. Cleland, Nature (London) **424**, 291 (2003).
[13]V. Sazonova, Y. Yaish, H. Ustunel, D. Roundy, T. A. Arias, and P. L. McEuen, Nature (London) **431**, 284 (2004); H. B. Peng, C. W. Chang, S. Aloni, T. D. Yuzvinsky, and A. Zettl, Phys. Rev. Lett. **97**, 087203 (2006).
[14]Y. T. Yang, K. L. Ekinci, X. M. H. Huang, L. M. Schiavone, M. L. Roukes, C. A. Zorman, and M. Mehregany, Appl. Phys. Lett. **78**, 162 (2001).
[15]S. Timoshenko, J. Opt. Soc. Am. **11**, 233 (1925).
[16]L. Jiang, R. Cheung, J. Hedley, M. Hassan, A. J. Harris, J. S. Burdess, M. Mehregany, and C. A. Zorman, Sens. Actuators, A **128**, 376 (2006); M. Zalalutdinov, K. L. Aubin, R. B. Reichenbach, A. T. Zehnder, B. Houston, J. M. Parpia, and H. G. Craighead, Appl. Phys. Lett. **83**, 3817 (2003).
[17]K. M. Jackson, J. Dunning, C. A. Zorman, M. Mehregany, and W. N. Sharpe, J. Microelectromech. Syst. **14**, 664 (2005).
[18]S. Dohn, R. Sandberg, W. Svendsen, and A. Boisen, Appl. Phys. Lett. **86**, 233501 (2005).